JCTC Journal of Chemical Theory and Computation

A Local Pair Natural Orbital Coupled Cluster Study of Rh Catalyzed Asymmetric Olefin Hydrogenation

Anakuthil Anoop,[†] Walter Thiel,[‡] and Frank Neese*,[†]

Institut für Physikalische und Theoretische Chemie, Wegelerstr 12, Bonn 53115 Germany and Max-Planck-Institut für Kohlenforschung, Kaiser-Wilhelm-Platz 1, Mülheim an der Ruhr, 45470 Germany

Received June 20, 2010

Abstract: The recently developed local pair natural orbital coupled cluster theory with single and double excitations (LPNO−CCSD) was used to study the rhodium-catalyzed asymmetric hydrogenation of two prochiral enamides. The method was carefully calibrated with respect to its accuracy. According to calculations on a truncated model system, the effects of perturbative triples (T) on the reaction energetics are very limited, the LPNO approximation is accurate, and complete basis set extrapolation (CBS) causes only minor changes in the relative energies computed with a standard basis set (def2-TZVP). The results for the full system are thus believed to be within 1−2 kcal/mol of the CCSD(T)/CBS limit for the present systems. Relativistic effects were treated by a scalar relativistic Hamiltonian using the zeroth order regular approximation (ZORA). The results of the study were compared to density functional calculations on the same systems and with calculations available in the literature. All calculations predict the correct stereochemical outcome of the reaction that is determined by the relative energies of the transition states in the early stages of the catalytic cycle. In general, DFT calculations using the B3LYP functional are in reasonable agreement with the LPNO−CCSD results, although deviations of 3−5 kcal/mol exist that are also not entirely systematic in the minor and major reaction branches. The present case study thus demonstrates that catalytic reactions, which are well described by single-reference electronic structure theory, can now be routinely studied with confidence in systems with 50−100 atoms applying local correlation methods that are as easy to use as DFT methods.

1. Introduction

New quantum chemical methods have to prove their utility in practical chemical applications. This is particularly true for local correlation approximations or otherwise simplified electron correlation methods where it is crucial that a consistent accuracy is maintained over the entire potential energy surface. Hence, species that differ in the number and nature of chemical bonds must be treated in a balanced way in order to obtain accurate results. At the same time, the methods should be easy to apply so that the user can focus attention on the chemical problem at hand rather than worry about technical details. Thus, it should not be necessary to readjust truncation parameters or to run long series of preliminary calculations.

According to previous test calculations, the newly developed local pair natural orbital coupled cluster method with single and double excitations (LPNO−CCSD)[1] is believed to fulfill these criteria. The method has three conservatively chosen truncation parameters and recovers 99.8−99.9% of the canonical CCSD correlation energy. It has been claimed that this accuracy will be generally reached and is not dependent on the particular chemical system or the basis set. In order to test whether the LPNO−CCSD method lives up to these ambitious expectations, we have chosen the Rh-based asymmetric hydrogenation as a subtle example of a

* Corresponding author phone: +49-228-732351, fax: +49-228-739064, e-mail: neese@thch.uni-bonn.de.

[†] Institut für Physikalische und Theoretische Chemie.

[‡] Max-Planck-Institut für Kohlenforschung.

10.1021/ct100337m
Published on Web 09/14/2010

transition-metal-catalyzed reaction.[2] In this catalytic cycle, there is a large number of intermediates and transition states. The outcome of the reaction depends on small energy differences between these species. Hence, it represents a challenging test case for the LPNO−CCSD method.

Besides balance, accuracy, and black-box character, another important aspect of actual chemical applications is the pronounced basis set dependence of electron correlation methods. The slow convergence of the correlation energy to the basis set limit is well-known and needs to be taken into account if comparison with experimental results is the goal. Unfortunately, most local correlation methods that have been developed to date increase dramatically in their computational cost if they are used in conjunction with at least triply polarized triple-ζ basis sets that probably represent the lowest basis set level at which one obtains reliable results. This is different for the LPNO methods that behave excellently with basis set extension such that calculations with extended basis sets remain affordable. Explicitly correlated local correlation methods may change this situation in the future.[3]

The asymmetric hydrogenation of prochiral olefins using Rh catalysts is the prototype of an enantioselective transition-metal-catalyzed reaction. It has received considerable interest both from theory and experiment because of its intriguing mechanistic aspects and its strong industrial and academic impact.[2b] Even though there are several successful catalysts for the efficient hydrogenation of several substrates, research efforts are continuing in this area due to the lack of a universal catalyst, and hence for each substrate an optimal catalyst has to be designed. The field has gained additional momentum from the discovery that highly enantioselective olefin hydrogenation can be achieved not only by the classic Rh catalysts with bidentate phosphorus ligands but also by Rh complexes containing BINOL-based monodentate ligands such as phosphites,[4] phosphonites,[5] and phosphoramidites.[6] For the classic catalysts with bidentate ligands, the major aspects of the mechanism appear to be well established by now,[7] and it is generally accepted that enantioselectivity results from kinetic control. That is, the minor diastereomer of the initially formed catalyst−substrate adduct reacts faster and thus yields the major product (anti-lock-and-key principle). By contrast, in the more recent catalysts with monodentate phosphorus ligands, there is evidence for the opposite behavior, with the major diastereomer leading to the favored enantiomeric product.[8] Computational studies of such subtle mechanistic issues require methods that are efficient enough to be applied to complex transition-metal systems, and at the same time accurate enough to unravel the specific features of any particular catalyst−substrate combination.

In this article, we have selected two classic examples of asymmetric Rh-catalyzed olefin hydrogenation that have been studied previously using a variety of methods including DFT and DFT/MM hybrid methods.[9,10] Since one of the major goals of the study is to compare local correlation with DFT methods, we focus on the established pathways in the catalytic cycle of two substrates, (a) α-formamidoacrylonitrile (hereafter called the cyano system)[9] and (b) N(1-*tert*-butylvinyl)formamide (hereafter called the butyl system).[10] The catalyst used in both reactions is [(*R*,*R*)-MeDuPHOS]$^+$ (Scheme 1).

Scheme 1. Asymmetric Hydrogenation of Enamides

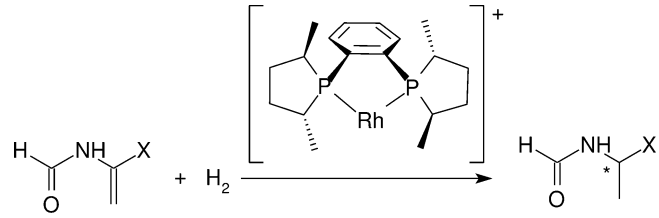

a) X = CN; b) X = *tert*-Bu

The generally accepted catalytic cycle (Scheme 2) involves the following elementary steps: (a) the formation of the diastereomeric catalyst−substrate adducts, (b) the addition of H_2 to the catalyst−substrate adduct, (c) the oxidative addition of H_2 to form the dihydride complex, (d) migratory insertion of the alkene into the Rh−H bonds in two consecutive steps, and (e) reductive elimination of the hydrogenated product.

Various reaction pathways originating from the different modes of coordination of the substrate to the catalyst and further from the different modes of addition of H_2 have been analyzed in detail by Feldgus and Landis.[9,10] In this study, we have included pathways that are important in the catalytic cycle. As shown by Feldgus and Landis, the enantioselectivity of these reactions is dominated by the reactivity of the catalyst−substrate adduct rather than by its stability.[9,10] The enantioselectivity and the rate-determining step have been shown to be variable and to depend on the specific combination of ligands and substrates.[9,10] The previous theoretical studies by Landis and co-workers have led to the conclusion that for the cyano and butyl systems investigated here, the rate-determining step is indeed the oxidative addition. Thus, the barriers toward the formation of the dihydride intermediates determine the enantioselectivity and are therefore of particular interest for the present study.

2. Computational Details

Density functional theory (DFT) was used for geometry optimizations. The optimizations for the butyl system were done by employing the BP86[11] functional in combination with the resolution of identity (RI) approximation[12] as implemented in Turbomole 5.71.[13] The Rh atom was described using the ecp-28-mwb[14] effective core potential and the associated basis set. All other atoms were described with the 6-31G*[15] basis set. Transition state optimizations were performed with ChemShell (version 3.0ac)[16] in conjunction with energy and gradient evaluations by Turbomole 5.71. For the cyano system, all optimizations were done using the ORCA program package[17] together with the RI-BP86 method (within the Split-RI-J variant[18]) and the segmented all-electron relativistically contracted (SARC[19]) TZVP basis set.[20] Unless otherwise stated, all ORCA calculations employed the scalar relativistic, all-electron ZORA approach in conjunction with the model potential idea of van Wüllen.[21]

Single-point energies for all species were computed with ORCA at various levels of theory. They include the DFT

Scheme 2. Catalytic Cycle for the Cyano System[a]

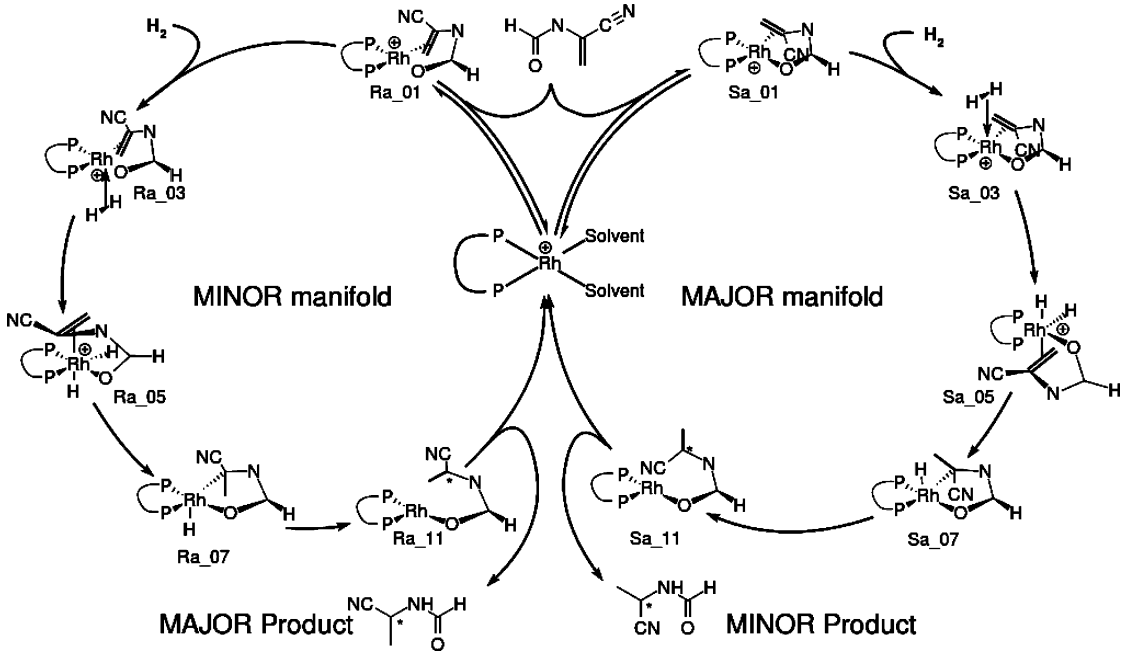

[a] One pathway each for the formation of *R* and *S* products is shown.

Scheme 3. Model System Used for the Calibration Study

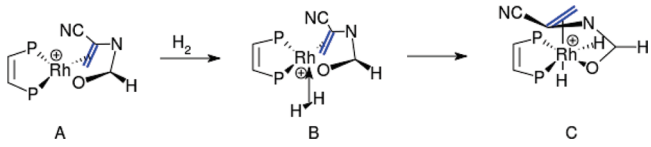

methods BP86 and B3LYP as well as the coupled cluster variants, CCSD, CCSD(T), LPNO−CCSD, LPNO−CEPA/1, and LPNO−QCISD.[1a] For B3LYP calculations, the RIJCOSX approximation[22] was applied. Ahlrichs basis sets of double-, triple-, and quadruple-ζ quality were used as described in the text. The truncation thresholds of the LPNO methods were left at their default values, $T_{\mathrm{CutPNO}} = 3.33 \times 10^{-7}$, $T_{\mathrm{CutPairs}} = 1 \times 10^{-4}$, and $T_{\mathrm{CutMKN}} = 1 \times 10^{-3}$.[1]

3. Results and Analysis

3.1. Calibration. For calibration purposes, the newly developed LPNO−CCSD approach was compared with canonical CCSD and CCSD(T) results. To this end, a truncated model system was constructed for which the bulkier substituents were replaced by hydrogen atoms (Scheme 3). The first two steps in the catalytic cycle of the minor manifold in the cyano system were modeled in this way. These two steps involve some of the more difficult bonding situations in the catalytic cycle. Since they also include some fairly major structural rearrangements (e.g., switch from a square planar to an octahedral rhodium species), these reaction steps should be representative of the entire catalytic cycle. The computed reaction and activation energies for the two steps are summarized in Table 1.

The Effect of Perturbative Triples. To study the influence of perturbative triple excitations, CCSD and CCSD(T) results were compared. In the canonical case, this can be done even for the small model system only in conjunction with a small basis set (def2-SVP). With the triples correction included, the exothermicity of the first step increases by 1.66 kcal/mol, and the second step becomes less endothermic by 0.64 kcal/mol. The activation energies are reduced by 0.49 and 0.93 kcal/mol, respectively. The negative activation barrier for the first step (−0.20 kcal/mol) is probably an artifact of the small basis set since the use of the TZVP basis set for the same step yields a positive barrier of 0.75 kcal/mol. We conclude that the effects of connected triples are fairly limited and can be disregarded in the present system. This is fortunate because an accurate (T) approximation has not yet been developed in the LPNO framework, and canonical calculations on the target systems with saturated basis sets are presently not feasible. We shall thus proceed with CCSD for the remainder of this study.

The Effect of LPNO Approximation. The errors arising from the LPNO approximation are found to be very small in our model system. The largest deviation from the canonical CCSD results is 0.28 kcal/mol, which can be considered negligible. This attests once more to the reliability of the LPNO approximation that has so far always faithfully reproduced the canonical coupled cluster results.

Basis Set Convergence. There are various procedures for the extrapolation to the complete basis set (CBS) limit. We have chosen to extrapolate the Hartree−Fock energy using[23]

$$E_{\mathrm{SCF}}^{(X)} = E_{\mathrm{SCF}}^{(\infty)} + A \exp(-\alpha\sqrt{X}) \qquad (1)$$

where $E_{\mathrm{SCF}}^{(X)}$ is the SCF energy for the basis set with cardinal number "*X*". We have employed the def2-TZVPP and def2-QZVPP basis sets for the extrapolation, and hence $X = 3$ and 4. $E_{\mathrm{SCF}}^{(\infty)}$ is the basis set limit SCF energy obtained with $\alpha = 7.88$, the optimized value for the def2 basis sets.[24]

Table 1. Reaction Energies and Activation Energies (kcal/mol) for the Model System (See Scheme 3)

		activation energy	reaction energy	activation energy	reaction energy
method	basis	A→B	A→B	B→C	B→C
BP86(RI)	def2-SVP	0.90	−7.20	4.02	2.30
B3LYP	def2-SVP	1.55	−2.71	6.17	3.79
CCSD	def2-SVP	0.29	−5.11	6.44	4.56
CCSD(T)	def2-SVP	−0.20	−6.77	5.51	3.92
CCSD(T)	ECP, TZVP	0.75	−6.09	5.80	4.52
LPNO−CCSD	def2-SVP	0.13	−4.83	6.48	4.44
LPNO−CCSD	def2-TZVPP	1.30	−3.17	6.53	4.36
LPNO−CCSD	def2-QZVPP	1.39	−3.34	6.56	4.33
LPNO−CCSD	CBS	1.36	−3.50	6.56	4.31
LPNO−CCSD	def2-TZVP	1.80	−3.04	6.70	4.67
LPNO−CCSD (full system)	def2-TZVP	2.07	−4.59	5.19	4.04
B3LYP(RIJCOSX)	def2-TZVP	2.75	−0.28	6.13	3.20
BP86(RI)	def2-TZVP	2.18	−4.38	3.93	1.48
BP86(RI)	CBS	1.84	−4.74	4.26	1.70
BP86(RI)	ECP,def2-TZVP	2.29	−4.14	4.28	1.86

For the extrapolation of the correlation energy, we use

$$E_{\mathrm{corr}}^{(\infty)} = \frac{X^{\beta}E_{\mathrm{corr}}^{(X)} - Y^{\beta}E_{\mathrm{corr}}^{(Y)}}{X^{\beta} - Y^{\beta}} \qquad (2)$$

with $\beta = 3.0$, which is the best choice for any combination of triple- and quadruple-ζ basis sets.[24,25] The extrapolation from the def2-TZVP basis to the CBS limit according to eqs 1 and 2 leads to overall changes of 0.46 and 0.36 kcal/mol in the reaction energies, and of 0.44 and 0.14 kcal/mol in the activation energies, respectively (Scheme 3). These changes are small, which indicates that def2-TZVP is an appropriate basis set for our purposes. Therefore, we have not applied any such extrapolation procedures in the remainder of this study.

Comparison of DFT and CCSD(T) (def2-SVP Basis). The BP86 and B3LYP results differ by 0.65 and 2.15 kcal/mol for the activation energies, and by 4.49 and 1.49 kcal/mol for the reaction energies. Compared to CCSD(T), the deviations are as follows: BP86 activation energies, 1.10 and 1.49 kcal/mol; BP86 reaction energies, 0.53 and 1.62 kcal/mol; B3LYP activation energies, 1.75 and −0.66 kcal/mol; B3LYP reaction energies, −4.06 and 0.13 kcal/mol. Thus, if CCSD(T) is accepted as a reference, the DFT errors are acceptably small. However, one should keep in mind that the basis set dependence is generally less pronounced for DFT than for CCSD(T), so that it is not clear whether the deviations between DFT and CCSD(T) will decrease or increase for larger basis sets.

Comparison of the Full System and the Truncated Model System. In the final step of the calibration, we checked that the use of a truncated model system does not affect our conclusions. Thus, we compared the energetics of the two investigated steps in the model system (Scheme 3) against those in the full system at the LPNO−CCSD/def2-TZVP level. The activation energy for hydrogen addition increased by merely 0.27 kcal/mol in the full system. Contrary to the expectations derived from steric arguments, the formation of the molecular hydrogen complex is *more* favorable for the full system by 1.55 kcal/mol. Similarly, the barrier for the oxidative addition is reduced in the full system by 1.51 kcal/mol. The formation of the dihydride complex is slightly less endothermic for the full system (0.63 kcal/mol). These changes are small enough to conclude that the validation achieved in the model system (with regard to perturbative triples, LPNO approximation, and basis set) will also hold for the full system. In an overall assessment, we thus expect that the deviations of the reported LPNO−CCSD results from the CCSD(T)/CBS limit are not larger than 1−2 kcal/mol.

3.2. Cyano System. We studied the two catalytically relevant pathways *R* and *S* that had previously been denoted as pathways **a** and **A**.[9] The energies of all species in the reaction cycle were calculated at the LPNO−CEPA/1, LPNO−QCISD, and LPNO−CCSD levels with the def2-TZVP basis set. The computed relative energies are given in Table 2 relative to Sa_01 + H_2, where Sa_01 denotes the *proS* conformer of the catalyst−substrate adduct (Scheme 2). The energy difference between the major (*proR*) and minor (*proS*) adducts is 3.24, 3.37, and 3.38 kcal/mol at the LPNO−CEPA/1, LPNO−QCISD, and LPNO−CCSD levels, respectively, in reasonable agreement with the DFT values of 2.30 (BP86) and 2.20 (B3LYP) kcal/mol and the B3LYP/ONIOM literature value[9] of 4.57 kcal/mol. The higher stability of the *proS* conformation (Sa_01) of the adduct compared to the *proR* conformation (Ra_01) is consistent with the experimental observation that the *proS* conformation is dominantly formed in solution.

In the following discussion, we focus on the computed energy profiles and disregard zero-point vibrational energies as well as finite-temperature and entropic effects. According to previous work,[9] the initial addition of molecular hydrogen is associated with a large entropic penalty, but there are only minor differences between the energies and the free energies at 300 K for the other reaction steps. In particular, these differences are very similar for corresponding steps on the *R* and *S* pathways so that we can assess the relative ease of the steps in the *R* and *S* manifold on the basis of the computed energy profiles. A quantitative evaluation of reaction rates would of course require the inclusion of zero-point, finite-temperature, and entropic corrections, which is beyond the scope of this article.

Given these caveats, the present calculations confirm that the *R* pathway is kinetically favored over the *S* pathway, since the highest point on the corresponding reaction profiles

Table 2. Relative Energies (kcal/mol) for the Hydrogenation of α-Formamidoacrylonitrile (Cyano System) Using [(*R*,*R*)-MeDuPHOS]$^{+a}$

molecule	BP86	B3LYP	LPNO−CEPA/1	LPNO−QCISD	LPNO−CCSD	B3LYP/ONIOM
Ra_01+ H_2	2.30	2.20	3.24	3.37	3.39	4.57
Ra_02	6.91	7.48	4.87	5.33	5.46	4.88
Ra_03	−0.40	3.66	−1.22	−1.01	−1.21	0.13
Ra_04	1.78	8.11	4.50	4.42	3.99	4.41
Ra_05	0.32	6.08	2.92	2.94	2.83	1.24
Ra_06	1.74	7.30	3.94	4.00	3.93	2.16
Ra_07	−6.94	−4.34	−8.78	−9.11	−9.14	−12.29
Ra_08	−5.32	−4.35	−9.22	−9.80	−9.88	−12.16
Ra_09	−19.19	−17.63	−21.06	−21.22	−21.52	−24.79
Ra_10	−5.94	−2.87	−4.54	−4.78	−4.55	−4.79
Ra_11	−24.78	−26.29	−25.57	−25.82	−25.49	−28.87
Sa_01 + H_2	0.00	0.00	0.00	0.00	0.00	0.00
Sa_02	9.89	10.81	8.62	9.26	9.36	9.67
Sa_03	3.44	7.38	3.16	3.50	3.33	5.24
Sa_04	5.24	11.23	8.27	8.30	7.95	8.95
Sa_05	2.41	7.81	4.89	5.02	5.00	5.74
Sa_06	4.48	9.79	7.02	7.14	7.13	5.89
Sa_09	−16.86	−15.26	−18.64	−18.74	−18.99	−22.37
Sa_10	−3.75	−1.38	−1.70	−1.92	−1.85	−2.67
Sa_11	−24.98	−26.30	−25.79	−25.95	−25.61	−29.23
Mean	0.19	−2.47	0.04	−0.04		0.92
rms	2.04	3.16	0.34	0.21		1.98
MAD	1.73	2.73	0.25	0.16		1.61
MAX	4.56	5.53	0.74	0.43		3.62

[a] The structures with odd numbers (e.g., Ra_01, Ra_03) represent minima (see Scheme 2), while the structures with even numbers (e.g., Ra_02, Ra_04) represent the intervening transition states. A statistical evaluation of the computed relative energies with respect to the LPNO−CCSD reference values provides the mean, root-mean-square (RMS), mean absolute (MAD), and maximum (MAX) deviations listed at the bottom. B3LYP/ONIOM data taken from Table 2 of ref 9.

is lower by 3.9 (LPNO−CCSD), 3.9 (LPNO−QCISD), 3.8 (LPNO−CEPA/1), 3.1 (B3LYP), 3.0 (BP86), and 4.8 kcal/mol (B3LYP/ONIOM[9]). In most cases (except for B3LYP), this is the transition state for the formation of the molecular hydrogen complex: the barrier for this process (relative to the catalyst−substrate adduct and H_2) is lower for the *R* pathway compared to the *S* pathway by 7.3 (LPNO−CCSD), 7.3 (LPNO−QCISD), 7.0 (LPNO−CEPA/1), 5.5 (B3LYP), 5.3 (BP86), and 5.7 kcal/mol (B3LYP/ONIOM[9]). The transition state for the subsequent oxidative addition (dihydride formation) has a similar energy that lies slightly below that of the initial transition state, typically within 1 kcal/mol (except for B3LYP, where it lies slightly higher, by less than 0.6 kcal/mol). These findings nicely explain why experimentally the *R* conformation of the final reaction product is formed in >99% enantiomeric excess. The higher activation energy found in the *S* pathway arises from the higher steric demand upon going from the square-planar catalyst−substrate adduct to the pentacoordinate molecular hydrogen complex and then to the dihydride. The proximity of the methyl group in the phosphine ligand to the substrate makes the transition state in the *S* pathway unfavorable relative to the one in the *R* pathway where the methyl group is rather distant from the substrate. This is a general feature of bidentate C_2 symmetric phosphine ligands which impose different steric demands on different enantiomeric pathways and thus facilitate chirality transfer.[2]

A statistical evaluation of the computed relative energies shows that LPNO−CEPA/1 and LNPO−QCISD reproduce the LPNO−CCSD reference values faithfully, with mean absolute deviations (MAD) of 0.25 and 0.16 kcal/mol, respectively, whereas BP86 and B3LYP show somewhat larger deviations (MAD of 1.73 and 2.73 kcal/mol). The maximum deviations are below 1 kcal/mol for the LPNO-based methods and around 5 kcal/mol for the DFT methods. Compared with LPNO−CCSD, the energies of the transition states and intermediates generally tend to be too low for BP86 and too high for B3LYP, by up to several kilocalories per mole. The deviations for B3LYP are reasonably systematic (see Figure 1), but not entirely uniform; for example, B3LYP underestimates the difference between the barriers for the initial hydrogen addition on the minor and major pathways by 2 kcal/mol, relative to LPNO−CCSD (see above). The deviations for BP86 are generally even less uniform (see Table 2).

3.3. Butyl System. We studied four catalytically relevant pathways which had previously been denoted as pathways **A** and **C** in the *R* and *S* manifolds.[10] The energies of all relevant species were computed at the BP86, B3LYP, LPNO−CEPA/1, and LPNO−CCSD levels. LPNO−QCISD calculations were not performed for the butyl systems since the LPNO−QCISD and LPNO−CCSD results had been very similar for the cyano system (Table 2). The calculated energies are given in Table 3 relative to Ra_01 + H_2.

Experimentally, the substitution of the cyano group in the substrate by a *tert*-butyl group (Scheme 1) changes the outcome of the reaction since it is exclusively the *S*-enantiomeric product that is observed in the butyl system (instead of the *R*-enantiomeric product in the cyano system). This has been rationalized previously[10] by a careful analysis of the possible stereochemical pathways for hydrogenation. Using the terminology introduced previously,[9,10] the favored mechanism involves pathway **C** in the butyl system and pathway **A** in the cyano system. These two pathways **A** and

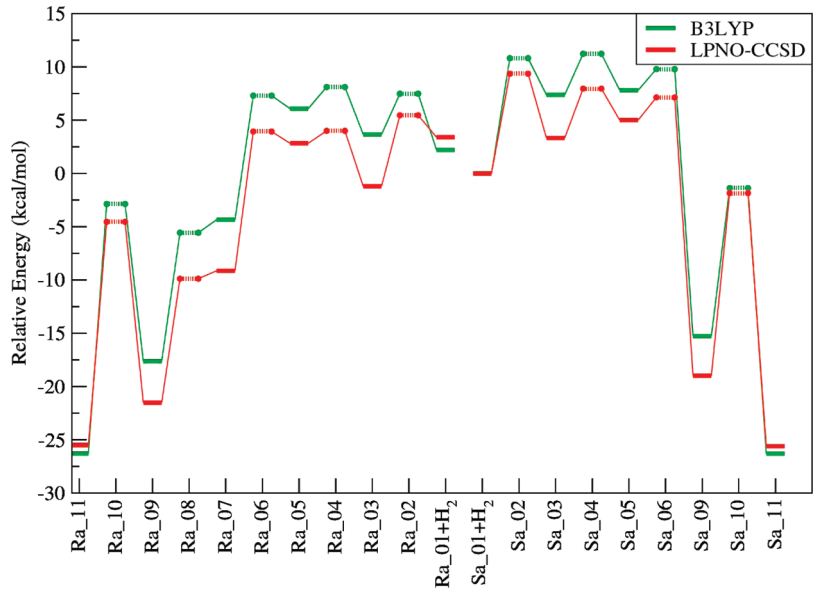

Figure 1. Reaction profile for the hydrogenation of α-formamidoacrylonitrile (cyano system) using [(*R*,*R*)-MeDuPHOS]$^+$ from B3LYP/def2-TZVP and LPNO−CCSD/def2-TZVP calculations.

C differ in the orientation of the incoming H_2 molecule with respect to the P−Rh−P plane and the C═C double bond of the substrate in the catalyst−substrate adduct. The geometry of this adduct is influenced by the substituents at the C═C double bond. The electron-deficient cyano group at the nonterminal α-carbon atom favors an orientation of the substrate with the terminal alkenyl carbon atom close to the P−Rh−P plane, whereas the *tert*-butyl group in the α position favors an orientation with the α-carbon close to this plane. The H_2 molecule prefers an approach from the side close to the terminal carbon (pathway **A**) in the former case and from the side of the nonterminal carbon (pathway **C**) in the latter case.

The *proR* conformer of the catalyst−substrate adduct has previously been found to be more stable than the *proS* conformer at the B3LYP/ONIOM level, but only by a small margin (0.46 kcal/mol).[10] This is confirmed by the present LPNO−CCSD, LPNO/CEPA-1, and B3LYP calculations that yield energy differences of 1.84, 1.26, and 0.10 kcal/mol, respectively, whereas BP86 gives the opposite stability order (*proS* more stable by 1.06 kcal/mol). At all levels applied, and in agreement with previous work,[10] pathway **C** in the *S* manifold is most favorable since the highest-energy barriers are much lower than those in the other pathways considered, because of less steric congestion.[10] In the present calculations, the highest point in the reaction profile of the favored pathway is reached at the transition state for the initial migratory insertion (Sc_06), which lies slightly above that for oxidative addition (Sc_04), by 1.2 (LPNO−CCSD), 1.2 (LPNO−CEPA/1), 0.6 (B3LYP), and 2.1 (BP86) kcal/mol, contrary to the B3LYP/ONIOM results where Sc_04 is highest in energy (0.3 kcal/mol above Sc_06). According to the current calculations, the best route to the *R* product also involves pathway **C**. The highest point of the energy profile corresponds again to the transition state for the initial migratory insertion (Rc_06), which lies 4.5 (LPNO−CCSD), 4.5 (LPNO−CEPA/1), 2.5 (B3LYP), and 2.4 (BP86) kcal/mol above Sc_06. The preference for enantioselective formation of the *S* product is thus more pronounced in the LPNO than in the DFT calculations. The B3LYP/ONIOM results[10] agree with the LPNO−CCSD results with regard to the predicted enantioselectivity since pathway **C** in the *S* manifold is favored by an even larger margin, but there are some discrepancies with regard to the other three pathways (Table 3): contrary to LPNO−CCSD, B3LYP/ONIOM prefers pathway **A** as the best route to the *R* product and gives different highest-energy transition states (Ra_04, Rc_04, and Sa_04 instead of Ra_06, Rc_06, and Sa_06, see Table 3), although it should be noted that the corresponding energy differences are not large.

The statistical evaluation of the computed relative energies confirms again that the LPNO−CEPA/1 results are close to the LPNO−CCSD reference values (MAD of 0.74 kcal/mol) while the DFT results are less reliable, with MAD values of 3.76 (2.22) kcal/mol and maximum deviations of more than 9 (5) kcal/mol for BP86 (B3LYP). Compared with LPNO−CCSD, the relative energies of the transition states and intermediates are generally underestimated by BP86. The corresponding B3LYP values are often in the right ballpark, especially in the mechanistically crucial first three steps of the reaction cycle, although they overestimate the LPNO−CCSD values by 2−4 kcal/mol in the case of the mechanistically most important pathway (see Table 3, from Sc_03 to Sc_06).

4. Conclusions

In this study, we have used recently developed local correlation methods to study a well established catalytic reaction cycle that involves subtle stereoelectronic effects. The validation for a truncated model system shows that the LPNO−CCSD approach faithfully reproduces the canonical CCSD results and that the effects of connected triple excitations are small. The LPNO−CCSD method is thus suitable for investigating such systems. It has been applied to compute energy profiles of the complete catalytic cycle for rhodium-catalyzed asymmetric hydrogenation of two

Table 3. Relative Energies (kcal/mol) for the Hydrogenation of (1-*tert*-butylvinyl)formamide (Butyl System) Using [(*R*,*R*)-MeDuPHOS]$^{+a}$

	BP86	B3LYP	LPNO−CEPA/1	LPNO−CCSD	B3LYP/ONIOM
Ra_01+ H_2	0.00	0.00	0.00	0.00	0.00
Ra_02	7.65	9.73	7.82	9.34	
Ra_03	4.39	9.87	7.10	8.04	11.18
Ra_04	8.40	16.73	15.34	15.59	15.08
Ra_05	0.61	1.35	7.85	6.69	0.83
Ra_06	8.49	15.09	14.22	14.37	9.47
Ra_07	−2.27	3.64	3.64	3.84	1.29
Ra_08	4.87	8.44	5.12	4.80	
Ra_09	−8.73	−6.00	−10.75	−11.43	−8.95
Ra_10	−0.34	3.81	3.33	2.92	
Ra_11	−26.87	−30.43	−26.15	−27.59	
Rc_02	1.95	4.84	5.39	6.08	
Rc_03	−2.17	3.55	2.36	2.67	8.09
Rc_04	0.56	9.26	9.96	9.90	17.70
Rc_05	1.82	1.08	5.94	4.70	−2.87
Rc_06	6.35	12.45	11.56	11.49	13.83
Rc_09	−17.31	−16.80	−12.67	−14.44	−15.48
Rc_10	−8.12	−6.53	−2.74	−4.31	
Rc_11	−23.22	−27.48	−23.68	−25.05	
Sa_01+ H_2	−1.06	0.10	1.26	1.84	
Sa_02	9.37	12.55	12.56	13.88	
Sa_03	6.62	12.36	11.41	12.34	19.18
Sa_04	12.15	20.45	19.12	19.35	25.16
Sa_05	0.22	0.97	7.10	5.95	0.38
Sa_06	10.69	17.70	18.98	19.40	15.41
Sa_07	5.44	10.85	8.32	8.92	7.25
Sa_08	6.42	11.04	8.00	7.83	
Sa_09	−10.99	−7.88	−10.63	−11.28	−7.95
Sa_10	1.01	4.93	3.48	3.09	
Sa_11	−27.03	−30.43	−26.96	−28.31	
Sc_02	0.80	3.49	2.33	2.98	
Sc_03	−4.41	1.27	−1.11	−0.91	2.37
Sc_04	1.82	9.53	5.87	5.75	7.53
Sc_05	−2.22	3.38	0.67	0.63	−2.66
Sc_06	3.96	10.09	7.10	6.99	7.20
Sc_09	−17.23	−16.62	−12.79	−14.52	−15.53
Sc_10	−11.87	−9.70	−2.91	−4.60	
Sc_11	−24.25	−27.22	−20.74	−22.39	
Mean	3.40	0.13	−0.27		−0.19
rms	4.41	2.70	0.94		4.18
MAD	3.76	2.22	0.74		3.50
MAX	9.34	5.43	1.77		7.80

[a] The structures with odd numbers (e.g. Ra_01, Ra_03) represent minima (Scheme 2), while the structures with even numbers (e. g. Ra_02, Ra_04) represent the intervening transition states. A statistical evaluation of the computed relative energies with respect to the LPNO−CCSD reference values provides the mean, root-mean-square (RMS), mean absolute (MAD), and maximum (MAX) deviations listed at the bottom. B3LYP/ONIOM data from Table 1 of ref 10.

prochiral enamide substrates. The calculations for the cyano and butyl systems are in qualitative agreement with experimental results in predicting the correct stereochemical outcome of the reaction in both cases. The qualitative picture is consistent with earlier studies that were done with density functional theory using the B3LYP/ONIOM approach.

The present B3LYP results are similar to those previously obtained by Landis and co-workers with B3LYP/ONIOM. Comparison of the B3LYP and LPNO−CCSD relative energies demonstrates mean absolute deviations of 2−3 kcal/mol (Tables 2 and 3). While this is in the realm commonly assumed for B3LYP, the deviations for individual reaction steps can be as large as 5 kcal/mol. In the case of BP86, the mean absolute deviations are 2−4 kcal/mol, and the maximum deviations range up to 9 kcal/mol in the butyl system. Moreover, the deviations between the DFT and LPNO−CCSD results are *not* constant over the potential energy surface (see the discussion in sections 3.2 and 3.3). These deviations should probably be considered as typical. They can be regarded as an indicator for the uncertainty in the computed DFT energies, since the results from high-level wavefunction based methods such as LPNO−CCSD are overall more reliable and more balanced.[26]

It is reassuring that all calculations reported here provide qualitatively consistent scenarios for the reaction mechanism and the same qualitative explanation for the origin of enantioselectivity. On the other hand, the significant and nonuniform differences between the DFT and LPNO−CCSD relative energies call for extreme caution in attempts to come up with quantitative predictions of enantioselectivity. According to rate theory, rather small changes in the computed barriers will result in significantly different relative reaction rates into the minor and major channels and will hence influence the relative amounts of minor and major reaction products formed. For example, in a single-step reaction with two competing paths for *R* and *S*, a difference of 1 (3) kcal/mol in the activation free energy between two paths gives rise to 69% (99%) enantiomeric excess. While it is not certain that the LPNO−CCSD energies are accurate enough for the reliable assessment of the relative rates in competing channels, it is clearly preferable to use them for this purpose (rather than DFT energies).

It may be considered as remarkable progress in theoretical methodology that calculations that had to be performed by an ONIOM-type DFT/MM approach with small basis sets 10 years ago can now be done in an all-electron scalar relativistic fashion with coupled cluster theory and large basis sets. We believe that this sets the stage for a more widespread use of the more generally reliable wave function-based *ab initio* technology in the study of catalytic reactions of industrial and biochemical relevance. Of high importance in this respect is the development of a consistent connected triples approximation in the LPNO framework as triples effects are often important for predicting accurate energetics. Efforts along these lines are underway in our laboratories.

Acknowledgment. We gratefully acknowledge the SFB 813 ("Chemistry at Spin Centers") for financial support of this work. A.A. thanks Martin Graf for helpful discussions.

References

(1) (a) Neese, F.; Wennmohs, F.; Hansen, A. *J. Chem. Phys.* **2009**, *130*, 114108–18. (b) Neese, F.; Hansen, A.; Liakos, D. G. *J. Chem. Phys.* **2009**, *131*, 064103−15.

(2) (a) de Vries, J. G.; Elsevier, C. J. *The Handbook of Homogeneous Hydrogenation*; Wiley-VCH: Weinheim, Germany, 2007. (b) Evans, P. A.; Tsuji, J. *Modern Rhodium-Catalyzed Organic Reactions*; Wiley-VCH: Weinheim, Germany, 2005.

(3) (a) Kutzelnigg, W. *Theor. Chem. Acc. (Theor. Chim. Acta)* **1985**, *68*, 445–469. (b) Marchetti, O.; Werner, H. J. *J. Phys. Chem. A* **2009**, *113*, 11580–11585. (c) Höfener, S.; Tew, D. P.; Klopper, W.; Helgaker, T. *Chem. Phys.* **2009**, *356*, 25–30.

(4) Reetz, M. T.; Mehler, G. *Angew. Chem., Int. Ed.* **2000**, *39*, 3889–3890.

(5) (a) Reetz, M. T.; Sell, T. *Tetrahedron Lett.* **2000**, *41*, 6333–6337. (b) Claver, C.; Fernandez, E.; Gillon, A.; Heslop, K.; Hyett, D. J.; Martorell, A.; Orpen, A. G.; Pringle, P. G. *Chem. Commun.* **2000**, 961–962.

(6) Van den Berg, M.; Minnaard, A. J.; Schudde, E. P.; van Esch, J.; de Vries, A. H. M.; Feringa, B. L. *J. Am. Chem. Soc.* **2000**, *122*, 11539–11540.

(7) Brown, J. M. Mechanism of Enantioselective Hydrogenation. In *The Handbook of Homogeneous Hydrogenation*; de Vries, J. G., Elsevier, C. J., Ed.; Wiley-VCH: Weinheim, Germany, 2007; p 1073.

(8) Reetz, M. T.; Meiswinkel, A.; Mehler, G.; Angermund, K.; Graf, M.; Thiel, W.; Mynott, R.; Blackmond, D. G. *J. Am. Chem. Soc.* **2005**, *127*, 10305–10313.

(9) Feldgus, S.; Landis, C. R. *J. Am. Chem. Soc.* **2000**, *122*, 12714–12727.

(10) Feldgus, S.; Landis, C. R. *Organometallics* **2001**, *20*, 2374–2386.

(11) (a) Becke, A. D. *Phys. Rev. A* **1988**, *38*, 3098. (b) Perdew, J. P. *Phys. Rev. B* **1986**, *33*, 8822.

(12) (a) Eichkorn, K.; Treutler, O.; Öhm, H.; Häser, M.; Ahlrichs, R. *Chem. Phys. Lett.* **1995**, *240*, 283–289. (b) Eichkorn, K.; Treutler, O.; Öhm, H.; Häser, M.; Ahlrichs, R. *Chem. Phys. Lett.* **1995**, *240*, 283–289. (c) Eichkorn, K.; Treutler, O.; Öhm, H.; Häser, M.; Ahlrichs, R. *Chem. Phys. Lett.* **1995**, *242*, 652–660.

(13) *TURBOMOLE*, V5.71; University of Karlsruhe and Forschungszentrum Karlsruhe GmbH: Karlsruhe, Germany, 2009. Available from http://www.turbomole.com (accessed Sep 2010).

(14) Andrae, D.; Häuβermann, U.; Dolg, M.; Stoll, H.; Preuβ, H. *Theor. Chem. Acc. (Theor. Chim. Acta)* **1990**, *77*, 123–141.

(15) Francl, M. M.; Pietro, W. J.; Hehre, W. J.; Binkley, J. S.; Gordon, M. S.; DeFrees, D. J.; Pople, J. A. *J. Chem. Phys.* **1982**, *77*, 3654–3665.

(16) (a) Sherwood, P.; de Vries, A. H.; Guest, M. F.; Schreckenbach, G.; Catlow, C. R. A.; French, S. A.; Sokol, A. A.; Bromley, S. T.; Thiel, W.; Turner, A. J.; Billeter, S.; Terstegen, F.; Thiel, S.; Kendrick, J.; Rogers, S. C.; Casci, J.; Watson, M.; King, F.; Karlsen, E.; Sjøvoll, M.; Fahmi, A.; Schäfer, A.; Lennartz, C. *THEOCHEM* **2003**, *632*, 1–28. (b) See http://www.chemshell.org (accessed Sep 2010).

(17) Neese, F. *ORCA*, version 2.7; University of Bonn: Bonn, Germany, 2010. http://www.thch.uni-bonn.de/tc/orca (accessed Aug 28, 2010).

(18) Neese, F. *J. Comput. Chem.* **2003**, *24*, 1740–1747.

(19) Pantazis, D. A.; Chen, X.; Landis, C. R.; Neese, F. *J. Chem. Theory Comput.* **2008**, *4*, 908–919.

(20) (a) Schäfer, A.; Horn, H.; Ahlrichs, R. *J. Chem. Phys.* **1992**, *97*, 2571–2577. (b) Weigend, F. *Phys. Chem. Chem. Phys.* **2006**, *8*, 1057–1065.

(21) van Wüllen, C. *J. Chem. Phys.* **1998**, *109*, 392–399.

(22) (a) Neese, F.; Wennmohs, F.; Hansen, A.; Becker, U. *Chem. Phys.* **2009**, *356*, 98–109. (b) Kossmann, S.; Neese, F. *Chem. Phys. Lett.* **2009**, *481*, 240–243.

(23) (a) Klopper, W.; Kutzelnigg, W. *THEOCHEM* **1986**, *135*, 339–356. (b) Kutzelnigg, W. *Int. J. Quantum Chem.* **1994**, *51*, 447–463. (c) Zhong, S. J.; Barnes, E. C.; Petersson, G. A. *J. Chem. Phys.* **2008**, *129*, 184116.

(24) Neese F. Unpublished results.

(25) Truhlar, D. G. *Chem. Phys. Lett.* **1998**, *294*, 45–48.

(26) Neese, F.; Hansen, A.; Wennmohs, F.; Grimme, S. *Acc. Chem. Res.* **2009**, *42*, 641–648.

CT100337M